Pertanika J. Sci. & Technol. 33 (2): 1049 - 1068 (2025)

PERTANIKA JOURNALS

SCIENCE & TECHNOLOGY

Journal homepage: http://www.pertanika.upm.edu.my/

A Novel Approach to Evaluating HEMA Polymer Gel Dosimeters Using Molecular Vibrational Features

Muhammad Alhassan[1,2]*, Azhar Abdul Rahman[1], Iskandar Shahrim Mustafa[1], Mohd Zahri Abdul Aziz[3], Mohd Zakir Kassim [3], Mohammed Salem Abdullah Bagahezel[3], Habib Ahmad Ibrahim[1] and Kabiru Alhaji Bala[1]

[1]School of Physics, Universiti Sains Malaysia, Main Campus, Pulau Pinang, Malaysia
[2]Department of Physics, Federal University Dutsin-Ma, 821101 Katsina State, Nigeria
[3]Department of Biomedical Imaging, Advanced Medical and Dental Institute, Universiti Sains Malaysia, Bandar Putra Bertam, 13200 Kepala Batas, Pulau Pinang, Malaysia

ABSTRACT

A polymer Gel Dosimeter (PGD) provides essential three-dimensional (3D) radiation dose distribution for the radiotherapy planning system (TPS). This study investigates the use of infrared absorption spectrum as a novel and more cost-effective alternative to Magnetic Resonance Imaging (MRI), Nuclear Magnetic Resonance (NMR), and Optical Computed Tomography (Optical CT) for reading out PGDs. The PGDs were fabricated using 2-Hydroxyethyl methacrylate (HEMA), maltose, N'N, methylene(bis)acrylamide (Bis), gelatin, deionized water (DI Water), and Tetrakis (hydroxymethyl) phosphonium chloride (THPC), and were irradiated using a Linear Accelerator (LINAC) within the range of 0–30 Gy. The possibility of translating molecular vibrational frequency, amplitude, and energy of vibration into absorbed dose was explored by analyzing the absorption spectra in the near-infrared region (NIR) with wavelengths between 750–1100 nm. The findings reveal that these vibrational properties can be employed to interpret irradiated PGDs. Furthermore, an increase in maltose concentration within the 0–520 mM range widens the linear dose range and enhances sensitivity. The PGDs exhibit temporal stability up to 7 days post-irradiation, and the span of their response remains relatively unaffected by scanning temperature. In conclusion, NIR spectroscopy offers a cost-effective method for interpreting PGDs, potentially improving the affordability and efficiency of PGD dosimetry in clinical radiotherapy. This holds particularly promising for less developed countries, aligning with the

ARTICLE INFO

Article history:
Received: 30 October 2023
Accepted: 3 October 2024
Published: 21 February 2025

DOI: https://doi.org/10.47836/pjst.33.2.23

E-mail addresses:
amuhammad@fudutsinma.edu.ng/amuhammad@student.usm.my (Muhammad Alhassan)
arazhar@usm.my (Azhar Abdul Rahman)
iskandarshah@usm.my (Iskandar Shahrim Mustafa)
mohdzahri@usm.my (Mohd Zahri Abdul Aziz)
mohdzakir@usm.my (Mohd Zakir Kassim)
msbagahezel@student.usm.my (Mohammed Salem Abdullah Bagahezel)
habibahmadibrahim@student.usm.my (Habib Ahmad Ibrahim)
kabala@student.usm.my (Kabiru Alhaji Bala)
*Corresponding author

ISSN: 0128-7680
e-ISSN: 2231-8526

sustainable development goal (SDG) of ensuring affordable healthcare for all. We finally recommend further research into translating the molecular vibrational parameters into 3D images.

Keywords: HEMA, infrared absorption spectrum, maltose additive, polymer gel dosimeter, saccharide additive

INTRODUCTION

Radiotherapy is a medical technique involving collective responsibilities among radiation oncologists, medical physicists, radiographers, and radiation technologists to eliminate cancerous cells in the human body using ionizing radiation. It becomes increasingly crucial with rising cancer incidences (Jaszczak et al., 2020). There are two common types of radiotherapy: internal radiotherapy or brachytherapy, which involves placing sealed radioisotopes near or inside the tumor (Shukor et al., 2022), and external beam radiotherapy, irradiating the tumor from outside the body. Precision in dosage prescription is paramount in radiotherapy, necessitating careful planning to ensure the target volume receives the proper dose without harming surrounding healthy tissues. As such, the need for a tool that could measure the dose distribution in a 3D manner arises (Kozicki et al., 2020). PGD is a tool made from hydrogels such as gelatin within which monomer is uniformly distributed and readily polymerizes on irradiation and is proven capable of measuring complex 3D radiation dose distribution with high precision and spatial resolution (Adliene et al., 2020; Jaszczak et al., 2020; Rabaeh et al., 2021; Shih et al., 2022).

On irradiation, radiation-induced polymerization occurs as a function of the absorbed dose in such a way that the level of polymerization could thereafter be translated into the absorbed dose (Mustaqim et al., 2020; Shih et al., 2022). Various physical and chemical changes in PGDs – such as shifts in transverse relaxation rate (R_2) during MRI, relaxation times during NMR, and optical appearances via optical CT scanning (OCS) could be translated into absorbed dose (Adliene et al., 2020; Jaszczak et al., 2020), alongside UV-visible spectrophotometry (UV-Vis) revealing optical changes and electronic transitions (Ishak et al., 2015), changes in CT number in x-ray CT scanning (Javaheri et al., 2020), and changes in speed of sound during Ultrasound scanning (Javaheri et al., 2020). Recent advancements utilize angular modulation, plasmonic sensors, and reflection intensity changes during Polarization-Sensitive Optical Coherence Tomography (PS-OCT) for evaluating polymerization (Adliene et al., 2020; Shih et al., 2022), with future predictions involving electrical impedance tomography (EIT), photoacoustic, and diffuse optical tomography (DOT) for PGD readouts (Deene, 2022). However, these techniques often rely on specialized machinery, posing obstacles to the realization of the sustainable development goal of providing comprehensive healthcare, especially in less developed countries.

Our present work pioneers translating molecular vibration-related changes in near infrared (NIR) absorption spectra into absorbed doses. The advantages of NIR spectroscopy

are the availability of infrared (IR) Spectrophotometer or Vis-IR spectrophotometer in most laboratories for identification of chemical substances, it is non-destructive, and is a fast technique compared to others (Masithoh et al., 2023; Zapata et al., 2021) and nowadays, some manufacturers such as Shimadzu, Japan manufactures UV-Vis spectrophotometers with extended energy range to NIR region and could be used to obtain absorption spectra and transmittance spectra of a sample within 200-1100 nm wavelength range. The utilization of UV-Vis spectrophotometer for PGD readout could be considered a better option due to its availability and cost-effectiveness (Lotfy et al., 2017).

The use of IR as a PGD readout technique hinges on the fact that irradiation-induced polymerization and crosslinking within the PGD lead to changes in molecular bonds (Deene, 2022), subsequently influencing the spectral position, bandwidth, and peak. These changes signify modifications in molecular vibration amplitude, frequency, and energy.

When a PGD is exposed to electromagnetic radiation (e.m. waves), three types of interactions can occur: (1) changes in rotational energy levels of molecules (this requires the least energy, typically at longer wavelengths), (2) changes in vibrational energy levels (this requires moderate energy, often happening in the NIR, and (3) electronic transitions (this requires the most energy, occurring at ultraviolet or visible wavelengths). While NIR is primarily associated with vibrational spectroscopy, it can also encompass electronic and rotational spectroscopies (Ozaki, 2021; Zapata et al., 2021). The spectral bands observed in the NIR are mostly due to functional groups containing hydrogen atoms, such as OH, CH, and NH, which are also present in this study's constituents of the PGDs.

In existing literature, IR spectrophotometers are employed in chemistry, biochemistry, biology, and material sciences to obtain transmittance or reflectance spectra within the 780–2500 nm range. These spectra are then translated into molecular vibrations for qualitative and quantitative analyses, determining the presence or concentration of specific materials, bonds, or functional groups in a sample (Darwish & Darwish, 2022; Pratiwi et al., 2022; Renner & Fritz, 2020; Zapata et al., 2021).

The scope of this study is limited to evaluating radiation-induced changes linked to molecular vibrations in the PGDs. Consequently, a single prominent absorption band within the NIR range is chosen to establish a connection between molecular vibrational changes and the absorbed dose that causes these changes. The limitation of this work and the usage of NIR for dose evaluation is the limited penetrability of IR, which might restrict its application in large PGD phantoms. Also, the shapes and sizes of sample holders in the present UV-Vis-IR spectrophotometers might restrict the evaluation of PGDs in humanoid phantoms.

This study aims to produce PGD using the less toxic monomer HEMA with a maltose additive. Subsequently, these PGDs will be irradiated with X-rays from a LINAC, and the vibrational parameters will be translated into absorbed doses.

MATERIALS AND METHOD

Gel Preparation

Four PGDs with varying maltose concentrations were prepared using the following components: DI Water (89.0%), gelatin (Type B, 225 g bloom) (6.0%), HEMA (2.7%), Bis (2.0%), and THPC (0.2%). All reagents except DI Water were obtained from Sigma-Aldrich, Germany. DI water was produced in the lab using the Arium® Pro water system machine.

The PGDs were prepared under normal atmospheric (normaxic) conditions (Nezhad et al., 2021). Throughout the PGDs' preparation, a hot plate with an integrated magnetic bar stirrer was used to facilitate the heating and stirring of the mixture. The PGDs were prepared by first heating DI water to 48°C to enable full dissolution of Bis. Following the addition of Bis, gelatin was added. The heating knob was switched off while the stirring continued to allow the mixture to cool. When the mixture became clear and transparent and cooled to 35°C, maltose was added, followed by HEMA and THPC at 27°C to avoid premature polymerization. The sequential addition of the components and the corresponding temperatures are outlined in Figure 1.

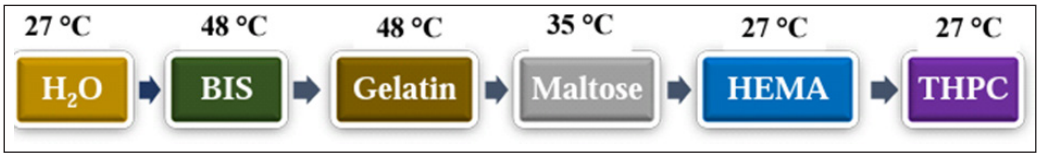

Figure 1. Preparation of PGD with the Sequential addition of its components

Following the addition of the last component, the PGDs' formulation was stirred for over 15 minutes at room temperature to ensure uniformity within the gel matrix. The mixture was then transferred to 4.5 cm^3 Perspex cuvettes with a 1.0 cm path length, tightly sealed with parafilm to prevent oxygen penetration, and placed in a refrigerator maintained at 4-6°C for gelation. These dosimeters are named here 'HEMAMAL' as an acronym for 'HEMA dosimeter + MALTOSE'; they are labeled as HEMAMAL1, HEMAMAL2, HEMAMAL3, and HEMAMAL4, corresponding to maltose concentrations of 0 mM, 80 mM, 230 mM, and 520 mM, respectively.

Irradiation

The PGDs were irradiated on the third day after manufacturing using an Elekta LINAC with a photon energy of 6 MV. The samples were positioned on a water phantom 5 cm thick and beneath another water phantom 1.5 cm thick, maintaining a source-surface distance (SSD) of 100 cm. This setup was within a 10 × 10 cm^2 field of view (FoV) in the isocenter. As mentioned elsewhere, the water phantom ensures uniform radiation distribution among

the PGDs, facilitates radiation build-up effects, and maintains scattering conditions (Al-jarrah et al., 2016).

The four batches of the PGD were irradiated to 5, 10, 15, 20, 25, and 30 Gy, while one PGD from each batch was left unirradiated (control sample). The arrangement for sample irradiation is illustrated in Figure 2.

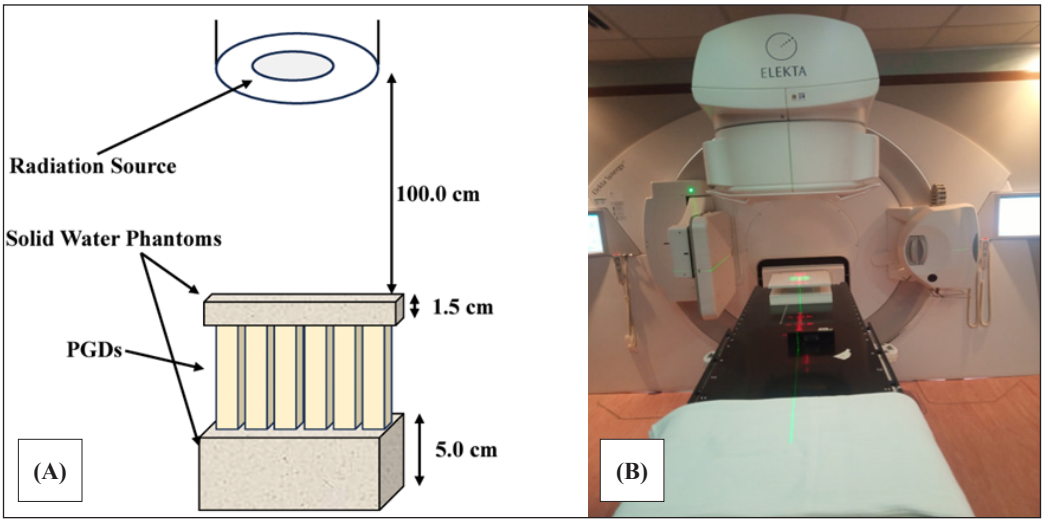

Figure 2. The visualization of irradiation setup with (A) The schematic diagram of the irradiation procedure and (B) Placement of PGDs at the isocenter of radiation FoV with the help of a laser beam

Dose Readout

The Shimadzu UV-1800 is a UV-Vis Spectrophotometer designed to scan samples across ultraviolet (UV), visible (Vis), and certain IR wavelengths. It can provide both absorption and transmittance spectra. Prior to the scanning process, the machine was allowed to warm up and complete initializations. Subsequently, it was configured for absorbance mode within the wavelength range of 750–1100 nm, a portion of the NIR spectrum (Ozaki, 2021). The scanning interval was set to be 1 nm at a medium scan speed, and the range of absorbance was 0.00–4.00. A Perspex cuvette almost full of DI water was used as the reference sample, and baseline correction was performed. The PGDs were scanned while maintaining the room temperature at 22.0 ± 0.5°C with the help of an air-conditioning system while the doors and windows remained closed.

In this study, we employed three principles to translate molecular vibrations into absorbed doses.

1. Relationship between Vibrational Amplitude and Concentration:
   This principle is rooted in Beer Lambert's law, which states the direct proportion between absorbance and concentration of the measured component (Equation 1):

$$A = \varepsilon lc \quad [1]$$

Where A represents peak absorbance or band intensity/amplitude, ε is the absorptivity, l is the optical path length, and c is the concentration (Darwish & Darwish, 2022; Pratiwi et al., 2022). In our case, concentration signifies polymerization levels and reflects the absorbed dose. Accordingly, we plotted graphs depicting changes in absorbance (ΔA) and peak absorbance (A_p) against absorbed dose.

2. Relationship between Absorbed Energy and Spectral Bandwidth:
Heightened polymerization necessitates greater energy to induce molecular vibrations from lower to higher energy states. This results from structural changes, viscosity changes, and changes in molecular conformity (Darwish & Darwish, 2022; Deene, 2004; Ishak et al., 2015). Energy and vibrational frequency are correlated through Equation 2:

$$E = h\nu \quad [2]$$

Where E is quantized energy, h is Planck's constant, and ν is the frequency (Abdel-Ghany et al., 2020; Ishak et al., 2015). If absorbed energy ΔE leads to an electronic transition or sets molecules into vibration, Equation 2 can be expanded to relate the energy to the absorbance bandwidth, as shown in Equation 3:

$$\Delta E = h\left(\nu_f - \nu_i\right) = hc\left(\frac{\Delta\lambda}{\lambda_f\lambda_i}\right) \quad [3]$$

Where $\nu_i = \frac{c}{\lambda_i}$ and $\nu_f = \frac{c}{\lambda_f}$ are initial and final vibrational frequencies before and after energy absorption, and Δλ is the bandwidth or the difference between λ_i and λ_f in cm. We plotted bandwidth against absorbed dose to capture this relationship.

3. Relationship between Energy and Molecular Frequency/Wave Number:
Equations 2 and 3 establish energy, vibration frequency, and wavelength connections. At λ_{max}, energy aligns with wave number ($\tilde{\nu}$) as shown in Equation 4:

$$E = hc\tilde{\nu} \quad [4]$$

Where $\tilde{\nu} = \frac{1}{\lambda_{max}}$ is the wave number and is measured in cm^{-1}.

Equation 5 defines the wave number for a harmonic oscillator, which is connected to the force constant of the molecular bonds and reduced mass.

$$\tilde{\nu} = \frac{1}{2\pi}\sqrt{\frac{k}{\mu}} \quad [5]$$

Where k represents the force constant in Ncm^{-1}, and μ is reduced mass in kg (Darwish & Darwish, 2022; Ozaki, 2021). In our case, varying polymerization levels and crosslinking lead to different concentrations of double bonds and functional groups within the irradiated polymer matrix. Consequently, different k and μ values emerge. Functional groups were also noted to influence PGD sensitivity to radiation (Deene, 2004). We plotted wavenumbers against absorbed dose to reflect this connection.

RESULT AND DISCUSSION

Absorption Spectra

The irradiated PGDs were scanned using a UV-Vis-IR spectrophotometer capable of covering a portion of the NIR spectrum. The dose evaluation was based on absorption spectra within the 750–1100 nm range, which are depicted in Figure 3.

The absorption spectra in Figure 3 (A)-(E) reveal distinct peak positions (λ_{max}) among the four PGDs. It is attributed to the influence of the maltose additive. This λ_{max} shift is also evident within each batch of PGDs irradiated at varying energies. This intra-batch shift is attributed to differing levels of polymerization and crosslinking, which impact molecular bond vibrations and can be correlated with absorbed doses causing polymerization and crosslinking. Figure 3(E), with an expanded view in 3(F), illustrates bandwidths of absorption spectra for HEMAMAL4 PGDs irradiated at 5, 10, 15, 20, 25, and 30 Gy doses. Bandwidths are measured at half peak absorbance ($\frac{1}{2}A_p$) for each spectrum. The accompanying table in Figure 3(F) indicates that bandwidth increases with an increase in absorbed dose.

Results in Figure 3(A)-(E) reveal the presence of multiple absorption bands with varying heights and widths attributed to diverse functional groups like OH, CH, and NH in dosimeter constituent components (Ozaki, 2021). These findings align with our expectation of λ_{max} shifting to higher energy (shorter wavelength) due to increased concentration of specific components, consistent with Beer Lambert's Law (Equation 1). These observations indicate the effect of absorbed dose on parameters associated with spectral height and width (Darwish & Darwish, 2022).

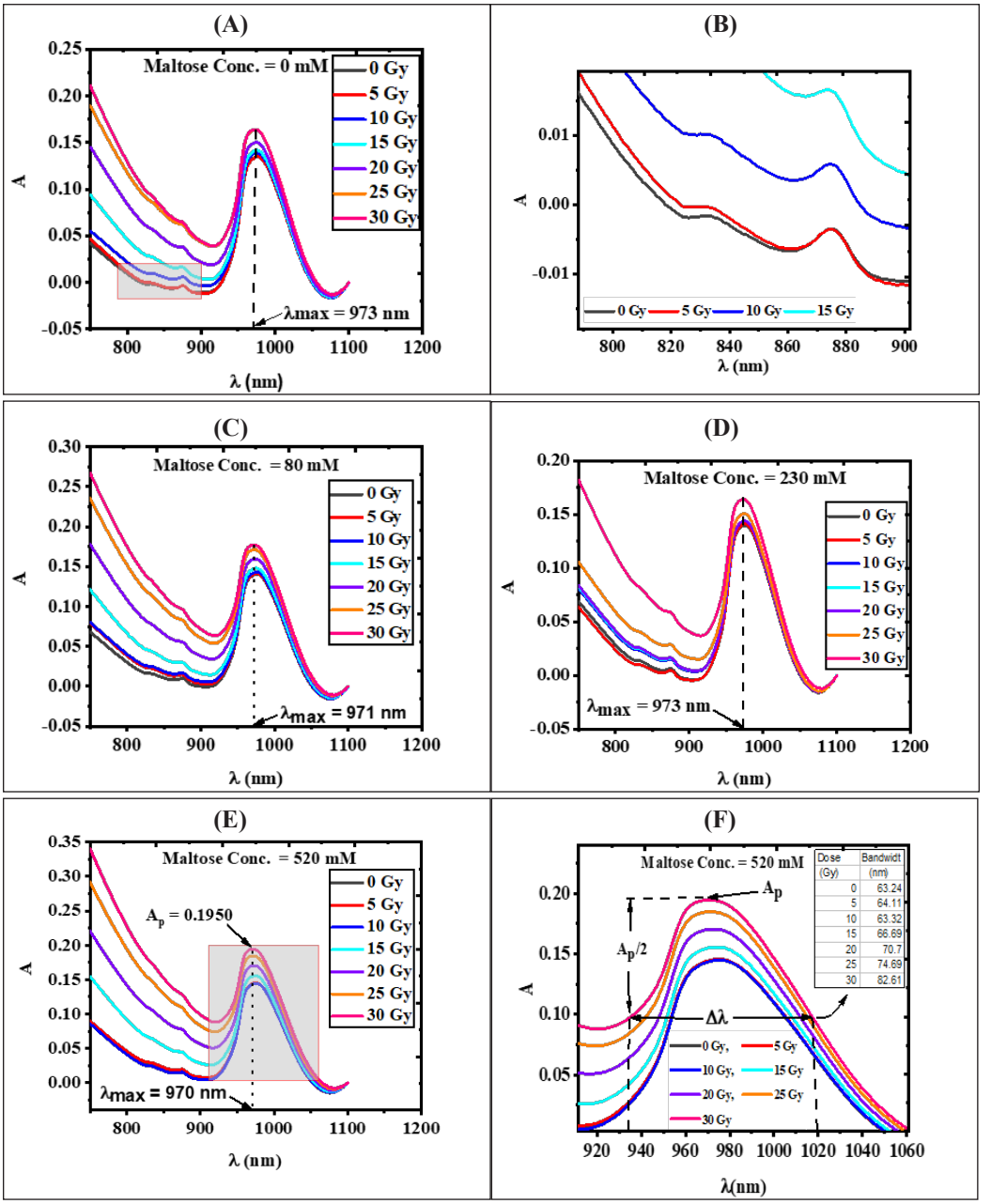

Figure 3. The absorption spectra of four PGDs (A) HEMAMAL1, (B) an enlarged portion of (A) as indicated by the arrow, (C) HEMAMAL2, (D) HEMAMAL3, (E) HEMAMAL4, and (F) an enlarged portion of (E) showing the bandwidth of HEMAMAL4, irradiated to 0-30 Gy

Dose-response

The dose-response, represented by (1) change in absorbance (ΔA), (2) peak absorbance (A_p), (3) bandwidth (Δλ), and (4) wave number ($\tilde{\nu}$), was plotted against the absorbed dose. The resulting graphs are displayed in Figure 4.

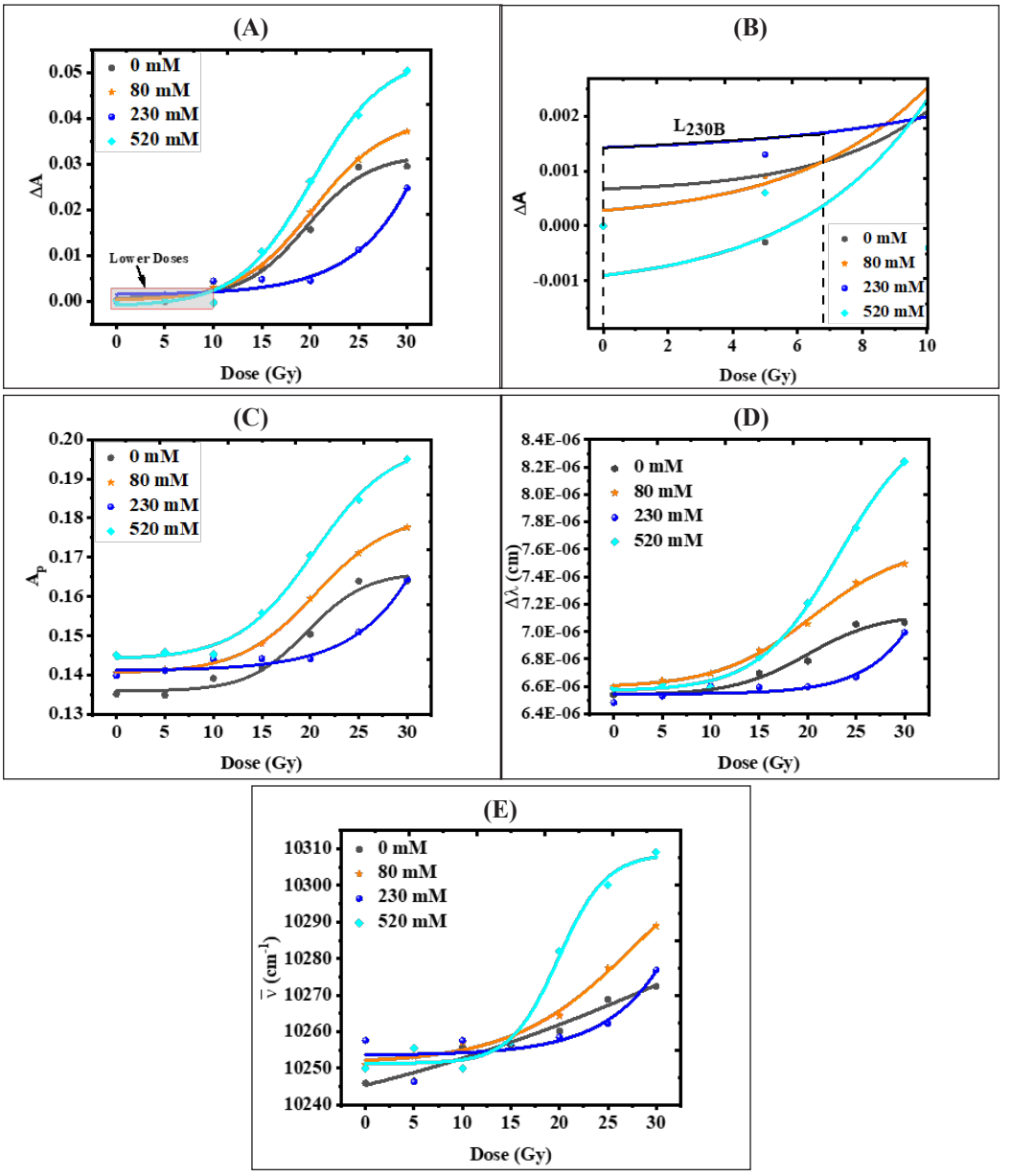

Figure 4. The relationship between the absorbed dose and the measured responses is (A) change in absorbance, (C) peak absorbance, (D) bandwidth, and (E) wave number. (B) is an enlarged portion of the lower dose region shown in (A)

The curves in Figure 4 (A)–(E) depict dose-response patterns for the four PGDs under investigation. These curves were fitted to sigmoidal dose-response curves and can be described mathematically using Hill's Equation, represented by Equation 6.

$$y = A_1 + \frac{A_1 + A_2}{1 + 10^{(Log_x 0 - x)p}} \quad [6]$$

In this equation, y represents the measured response, x represents the dose, A_1 and A_2 denote the lower and upper response limits, and p indicates the slope measured at the steepest point ($x = \log_x 0$, and $y = \frac{A_1 + A_2}{2}$) (Gadagkar & Call, 2015).

The findings in Figure 4(A)–(E) demonstrate gradual response increments at lower doses, followed by more substantial and linear increments at higher doses. As the dose approaches 30 Gy, the response tends to slow again. These graphs highlight that the lower dose range, the extent of the linear region, and the point where responses slow down a second time vary with the response type and the amount of maltose present in each dosimeter. For instance, the linear dose ranges for HEMAMAL1, HEMAMAL2, HEMAMAL3, and HEMAMAL4 are approximately 14.80–24.60 Gy, 14.20–25.70 Gy, 27.00–30.00 Gy, and 14.20 Gy–25.80 Gy, respectively. Comprehensive ranges for all PGDs based on the four different response types used in this study, along with the correlation coefficient (R^2) for each, are presented in Table 1.

The nonlinearity observed in the response of PGDs at lower doses compared to higher doses is attributed to a mechanism that remains not fully understood (Adliene et al., 2020). However, it is suggested that inhibitors such as oxygen could form peroxide radicals, which can potentially terminate the polymerization reaction at lower doses. In contrast, the polymerizing system has a higher viscosity at higher doses, facilitating interactions between growing polymer chains. This impedes termination by inhibitors and results in a steeper response (Deene, 2004). Nevertheless, linearity can still be achieved at lower doses, as illustrated in Figure 4(A), the magnified section in 4(B), and 4(C)–(D), where HEMAMAL3 exhibits linear dose-response within the 0-6 Gy range. However, the gradient is comparatively lower than at higher doses (Deene, 2004).

Similar cases to this observation have been documented in the literature. For instance, the Fricke-xylenol orange (FXO) gel dosimeter, evaluated using Optical CT, displays linearity within the 1–8 Gy range and becomes sublinear for doses below or above this interval (Nezhad & Geraily, 2022). BANG PGD, as manufactured by Farajollahi et al. (1999), also demonstrates a linear region up to 10 Gy (Nezhad & Geraily, 2022). In our study, the linear regions of the dosimeters start from doses around 13.6 Gy, with varying ranges of linearity spanning 2.7–30 Gy, as detailed in Table 1. This variation arises from differences in maltose content within each PGD and the specific response type being measured. Such observations are unsurprising, as reported linear dose ranges

in existing literature are dependent upon PGD's composition, irradiation techniques, and scanning techniques. For example, the PAMPSGAT PGD prepared from 2-Acrylamido-2-MethylPropane Sulfonic acid (AMPS), and scanned via MRI, exhibits a linear dose range within 10–40 Gy (Rashidi et al., 2020). Similarly, NIBMAGAT, synthesized from N-(Isobutoxymethyl) acrylamide monomer and evaluated through UV-Vis readout and NMR, demonstrates linearity within 5–20 Gy, with a linear range of 15 Gy (Lotfy et al., 2017). VIPAR dosimeter, evaluated by Kipouros et al. (2001), is reported to maintain linearity up to 40 Gy (Nezhad & Geraily, 2022).

Table 1
The linearity and correlation coefficients of fitting to the sigmoidal dose-response curve of the four PGDs under study, with different types of responses, are shown

Type of Response	Maltose Conc. (mM)	D_1 (Gy)	D_2 (Gy)	Linearity (Gy)	R^2
ΔA	0	14.80	24.60	9.80	0.9840
	80	14.20	25.70	11.50	0.9997
	230	27.00	30.00	3.00	0.9792
	520	14.20	25.80	11.60	0.9957
A_p	0	15.20	24.20	9.00	0.9834
	80	15.30	25.70	10.40	1.0000
	230	25.70	30.00	4.30	0.9817
	520	14.70	26.00	11.30	0.9964
$\Delta\lambda$	0	14.20	26.70	12.50	0.9792
	80	13.60	27.80	14.20	0.9953
	230	27.00	30.00	3.00	0.9489
	520	17.30	28.10	10.80	0.9840
$\tilde{\nu}$	0	0.00	30.00	30.00	0.9643
	80	19.30	30.00	10.70	0.9920
	230	27.30	30.00	2.70	0.8253
	520	16.00	24.10	8.40	0.9616

D_1 = beginning of the linear dose region, D_2 = end of the linear dose region, and R^2 = correlation coefficient

Unlike other PGDs, HEMAMAL1, depicted in Figure 4(E), demonstrates fitting to both sigmoidal dose-response curve ($R^2 = 0.9643$) and linear curve ($R^2 = 0.9578$) within the 0–30 Gy range, based on changes in bandwidth. It displays a gradient of 0.9152 $cmGy^{-1}$. Similarly, the VIPET dosimeter was reported to exhibit wide linearity up to 30 Gy before saturation, based on R_2-dose response (Watanabe et al., 2022).

The outcomes in Table 1 show the broadening of the linear region with increasing maltose concentration, except for HEMAMAL3, based on changes in absorbance and peak absorbance responses. This reveals maltose's ability to enhance HEMA PGD's linear

range. The effect of maltose concentration in elevating peak absorbance and shifting λ_{max} at doses of 5, 10, 15, 20, 25, and 30 Gy is depicted in Figure 5(A) and (B), respectively.

Combining the curves in Figure 4(A)-(E) with Table 1 reveals a robust correlation between absorbed dose and change in absorbance (ΔA) (R^2 = 0.9840, 0.9997, 0.9792, and 0.9957 for HEMAMAL1, HEMAMAL2, HEMAMAL3, and HEMAMAL4 respectively). Similarly, correlations are evident for peak absorbance (R^2 = 0.9834, 1.0000, 0.9817, and 0.9964), bandwidth (R^2 = 0.9792, 0.9953, 0.9489, and 0.9840), and wave number (R^2 = 0.9643, 0.9920, 0.8253, and 0.9616). The bandwidth ($\Delta\lambda$) signifies the energy range of molecular vibration, as shown in Equation 3, while the wave number ($\tilde{\nu}$) represents molecular vibration frequency, as illustrated in Equations 2–4. These correlations hint at the potential utilization of various energy aspects of molecular vibration (spectral bandwidth), intensity/amplitude (peak absorbance), and frequency (wave number) for translating into absorbed doses.

Effect of Maltose Concentration on Radiation Dose Response

Maltose concentration is observed to impact the response of the studied PGDs, as evident in Figures 4(A)—(E) and Table 1. The impact across varying absorbed dose levels is illustrated in Figures 5(A) and 5(B) based on peak absorbance (A_p) and λ_{max}, respectively.

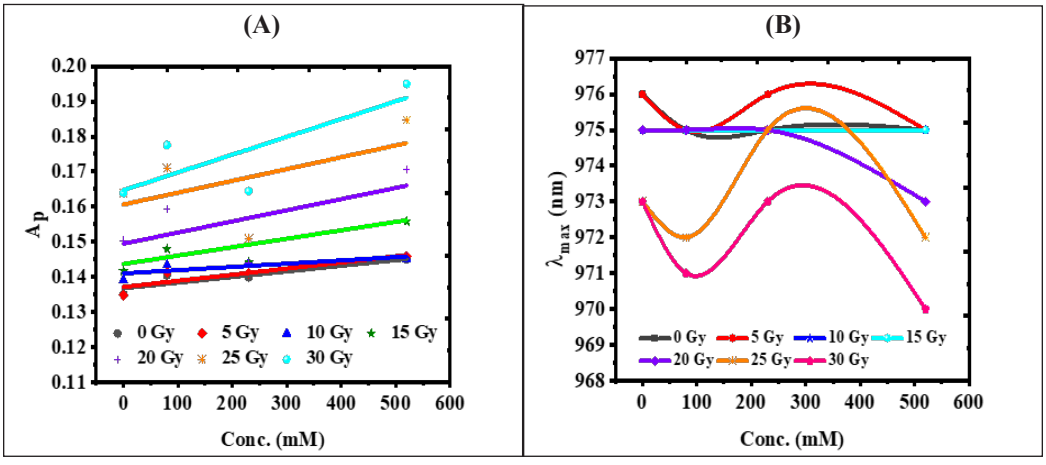

Figure 5. The effect of maltose concentration (A) to increase the peak absorbance and (B) to shift the λ_{max} for absorbed doses of 5, 10, 15, 20, 25, and 30 Gy

An increase in A_p and a decrease in λ_{max} serve as indicators of increased polymerization within the PGD. The overlap between the curves for 10 Gy and 15 Gy and the curve for 0 Gy, as observed in Figure 5(B), can, therefore, suggest a deceleration in polymerization when the absorbed dose exceeds 5 Gy until 15 Gy, beyond which there is a resurgence in polymerization rate, as evident from the curves for 20 Gy, 25 Gy, and 30 Gy.

Sensitivity

Sensitivity is a key characteristic of PGDs that reflects their ability to respond to radiation. It is determined by the ratio of the change in response to the change in dose, represented by the slope of the linear portion of the fitting curve (Bahrami et al., 2021; Deene, 2004). The sensitivities of four PGDs, namely HEMAMAL1, HEMAMAL2, HEMAMAL3, and HEMAMAL4, sharing the same composition except for maltose concentrations irradiated within the 0-30 Gy range, are illustrated in Figure 6 based on changes in absorbance, bandwidth, peak absorbance, and wave number.

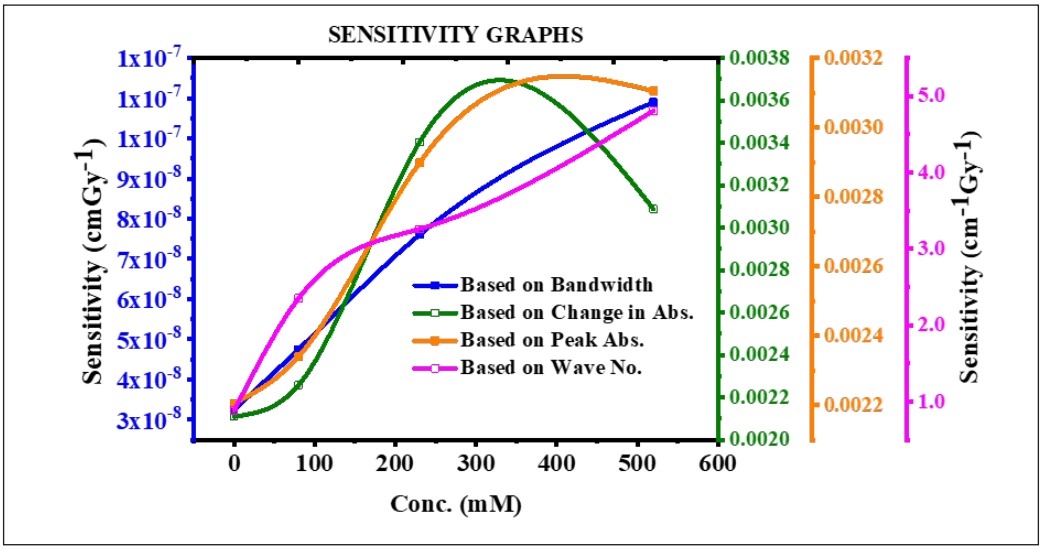

Figure 6. The sensitivity of HEMA PGDs as a function of maltose concentration is based on various measured responses

The findings in Figure 6 reveal an increase in sensitivity with rising maltose concentration. Notably, sensitivities differ across various response types, each carrying its own unit. For bandwidth measured in cm, sensitivity is expressed as $cmGy^{-1}$. In terms of bandwidth, sensitivity increases with maltose concentration up to 520 mM. Sensitivity calculated based on wave number (measured in cm^{-1}) is also expressed in $cm^{-1}Gy^{-1}$. In this context, wave number sensitivity gradually increases within 100-200 mM and a more substantial increase or steeper curve within maltose concentrations of 0-100 mM and 200-520 mM.

Sensitivities based on peak absorbance and change in absorbance are derived from the slope of Beer Lambert's law in equation 1, and they share the unit ($cm^{-1}Gy^{-1}$). These two responses reveal sensitivities reaching peak values of 0.0037 $cm^{-1}Gy^{-1}$ at 329 mM and 0.0032 $cm^{-1}Gy^{-1}$ at 406 mM for change in absorbance and peak absorbance responses,

respectively, after which they begin to decline. In parallel, we are concurrently pursuing research to determine the optimal maltose concentration for HEMA PGD, utilizing the UV-Vis readout technique and exploring various options for baseline correction and reference samples.

This outcome underscores the dependence of the sensitivity of PGDs on the composition of their components and the readout technique employed. In a previous study, NIBMAGAT gel dosimeters irradiated within the 0-30 Gy range exhibited a sensitivity of 0.016 $cm^{-1}Gy^{-1}$ based on UV-Vis readout and 0.0775 $s^{-1}Gy^{-1}$ based on NMR (Lotfy et al., 2017). Notably, sensitivity based on UV-Vis can also vary for the same dosimeter, depending on the λ_{max}. As an example, the sensitivity of HEMATAG PGD, composed of HEMA as the monomer, was reported as 0.017, 0.015, 0.013, 0.011, and 0.006 $cm^{-1}Gy^{-1}$ at λ_{max} = 500, 550, 600, 650, and 700 nm respectively (Ishak et al., 2015).

Temporal Stability

A study on the stability of PGD responses after irradiation reveals the continuation of polymerization for several hours. It is attributed to the net flux of fresh monomers from regions of low dose to regions of high dose, where they react with long-living polymer radicals in that region. It can also result from auto-polymerization of monomers or structural changes in the gel matrix. However, this effect is unwanted as it could lead to overestimating the absorbed dose (Aliasgharzadeh et al., 2022; Deene, 2004). The temporal stability of HEMAMAL2 was evaluated and is presented in Figure 7.

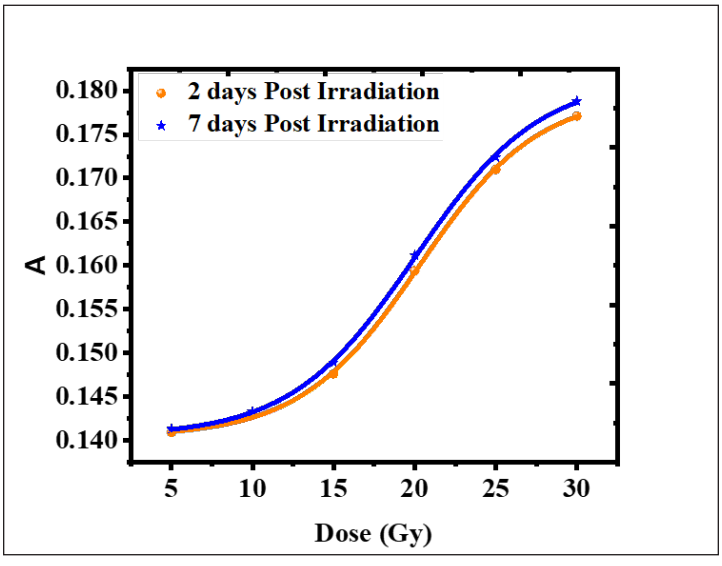

Figure 7. The response of HEMAMAL2 scanned 2 days and 7 days after irradiation

Figure 7 depicts the response curves of HEMAMAL2 scanned 2 days and 7 days post irradiation. These two curves are compared based on the parameters A_1, A_2, $\log_x 0$, and p, which describe the sigmoidal dose-response curve given in Equation 6. The comparison results are presented in Table 2.

Table 2
Comparison between the various parameters of HEMAMAL2 scanned 2 days and 7 days post-irradiation

Post Irrad.	A_1	A_2	$\text{Log}_x 0$	p ($cm^{-1}Gy^{-1}$)	R^2
2 days	0.1404	0.1796	20.3020 ± 0.17	0.1291 ± 0.01	0.9998
7 days	0.1405	0.1815	20.0347 ± 0.20	0.1134 ± 0.01	0.9995
|Dev.|	0.0001	0.0019	0.2673	0.0057	
%Dev.	0.0712%	1.0579%	1.3166%	4.7859%	

Post Irrad. = Post irradiation time, Dev. = deviation, and %Dev. = Percentage deviation

Table 2 shows that the change in absorbance scanned 7 days post-irradiation deviated from its response 2 days post-irradiation by approximately 0.07% in A_1, 1.1% in A_2, 1.3% in $\log_x 0$, and 4.8% in p. The standard errors in A_1 and A_2 are in the order of 10^{-4} and are thus considered negligible. This outcome is consistent with temporal stability up to 8 days post-irradiation based on transverse relaxation rate (R_2) and optical absorbance readout techniques reported in another study (Lotfy et al., 2017). Similar stability was observed in the PAKAG PGD 7 days post-irradiation (Rashidi et al., 2020).

Temperature Independence

Temperature can significantly impact the response of irradiated PGDs. This effect may stem from a decrease in viscosity as temperature rises (Deene, 2004). The impact of scanning temperature on HEMAMAL2's response was assessed at two distinct temperatures: 22°C and 25°C, as illustrated in Figure 8.

The two curves in Figure 8 are comparable based on values like A_1, A_2, $\log_x 0$, p, and R^2, provided in Table 3.

Table 3
Comparison between the response of HEMAMAL2 scanned at 22°C and at 25°C

Scan. Temp.	A_1	A_2	$\text{Log}_x 0$	p ($cm^{-1}Gy^{-1}$)	R^2
22°C	0.1288	0.1678	17.6639 ± 4.6892	0.0872 ± 0.1063	0.9267
25°C	0.1312	0.1670	16.0286 ± 4.8687	0.1099 ± 0.1731	0.8680
|Dev.|	0.0024	0.0008	1.6353	0.0227	
% Dev.	1.8634%	0.4768%	9.2579%	26.0321%	

Scan. Temp. = Scanning Temperature

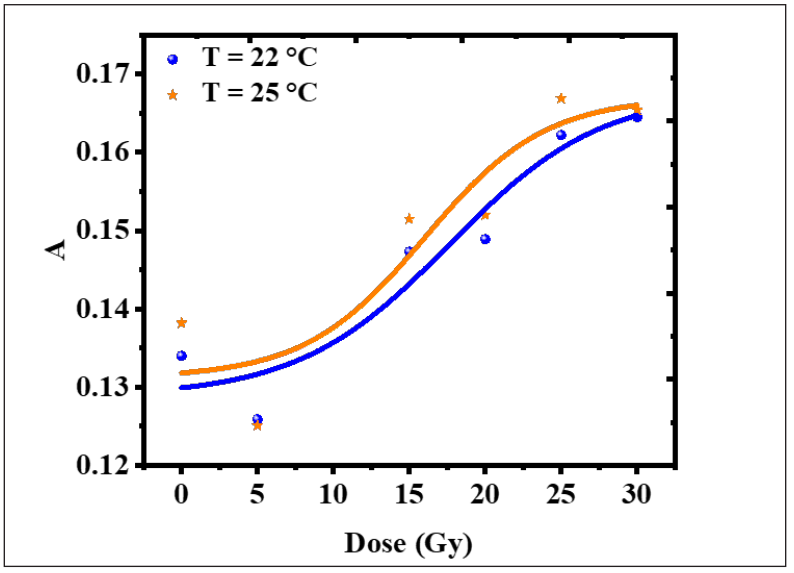

Figure 8. The sigmoidal dose-response curves of HEMAMAL2 scanned at 22°C and 25°C based on absorbance

The examination of Table 3 reveals differences in the lower and upper asymptotes A_1 and A_2 at 22°C and 25°C, which are approximately 1.9% and 0.5%, respectively. The SE values for A_1 and A_2 are 10^{-3} and thus not deemed significant. It suggests relative stability in the span of the dosimeter's response at both temperatures. This finding aligns with the stability observed in the PASSAG gel dosimeter's response, as measured by R_2 when scanned within the temperature ranges of 15°C–18°C and 20°C–24°C (Aliasgharzadeh et al., 2022).

However, the sensitivity (p) at 25°C deviates by 0.0227 $cm^{-1}Gy^{-1}$ (approximately 26.0%) from that at 22°C. This discrepancy can be attributed to the shifting back of the steepest point on the curve to lower dose by 1.6 Gy when scanned at 25°C compared to 22°C, owing to the nature of the Hill's curve. This shift likely arises from structural change or increased mobility of the polymerized and crosslinking molecules at higher temperatures, as this significantly affects the PGD's dose response (Deene, 2004).

Applicability of NIR for PGD Evaluation in Clinical Settings and Future Research

NIR spectroscopy can practically be employed for PGD evaluation in clinical settings by installing a high-quality UV-Vis-IR spectrophotometer with a sample holder suitable for various shapes and sizes of phantoms. Some manufacturers have recently provided two or more sample holders that can be substituted for various shapes and sizes. The device shall be accurately calibrated, evaluated and standardized for consistent dose evaluation.

Future research on translating molecular vibrational parameters into 3D images could involve inventing NIR spectral analysis software and algorithms to be integrated into imaging devices or real-time displays that can correlate molecular vibrational changes with the absorbed dose to map 3D dose distribution. Although this could be more complex than ordinary UV-Vis-IR spectroscopy, it might be less time-consuming and more cost-effective.

CONCLUSION

HEMA-based PGDs with maltose additive were fabricated, irradiated within the 0–30 Gy range, and subsequently scanned using a UV-Vis-IR spectrophotometer spanning 750–1100 nm. The outcomes demonstrated the feasibility of translating molecular vibrational frequency, amplitude/intensity, and vibration energy into absorbed doses. The linear dose range and sensitivity expanded as maltose concentration increased. The PGDs' response remained stable for up to 7 days post-irradiation, and this stability was relatively unaffected by scanning temperature. In conclusion, IR spectroscopy presents a potentially more cost-effective means of reading HEMA PGDs. Furthermore, the addition of maltose within the range of 0–520 mM exhibited the capacity to enhance both sensitivity and linear dose responses of the PGDs. These findings promise to enhance the affordability of radiotherapy procedures for underserved populations while bolstering the efficiency of PGD dosimetry in clinical radiotherapy. We finally recommend further research into translating the molecular vibrational parameters into 3D images.

ACKNOWLEDGEMENT

We appreciate the account of the Postgraduate Grant, School of Physics, USM (No Akaun: 308.AIFIZIK.415403) for financial support to purchase reagents. We also extend our gratitude to the technical assistance provided by the Department of Biomedical Imaging, Advanced Medical and Dental Institute, USM, Mr. Mohd Rizal Mohammad Rodin, and Mr. Hazhar Hassan, both from the School of Physics, USM.

REFERENCES

Abdel-Ghany, A. M., Abu-Khadra, A. S., & Sadeq, M. S. (2020). Influence of Fe cations on the structural and optical properties of alkali-alkaline borate glasses. *Journal of Non-Crystalline Solids*, *548*, Article 120320. https://doi.org/10.1016/j.jnoncrysol.2020.120320

Adliene, D., Urbonavicius, B. G., Laurikaitiene, J., & Puiso, J. (2020). New application of polymer gels in medical radiation dosimetry: Plasmonic sensors. *Radiation Physics and Chemistry*, *168*, Article 108609. https://doi.org/10.1016/j.radphyschem.2019.108609

Al-Jarrah, A. M., Rahman, A. A., Shahrim, I., Razak, N. N. A. N. A., Ababneh, B., & Tousi, E. T. (2016). Effect of inorganic salts and glucose additives on dose–response, melting point and mass density of genipin gel dosimeters. *Physica Medica*, *32*(1), 36–41. https://doi.org/10.1016/j.ejmp.2015.09.003

Aliasgharzadeh, A., Anaraki, V., Khoramian, D., Ghorbani, M., & Farhood, B. (2022). The impact of various amounts of fabricating components on the response of PASSAG polymer gel dosimeter: An optimization study. *Radiation Physics and Chemistry*, *190*, Article 109804. https://doi.org/10.1016/j.radphyschem.2021.109804

Bahrami, F., Abtahi, S. M. M., Sardari, D., & Bakhshandeh, M. (2021). Investigation of a modified radiochromic genipin-gel dosimeter: Dosimetric characteristics and radiological properties. *Journal of Radioanalytical and Nuclear Chemistry*, *328*(1), 19–31. https://doi.org/10.1007/s10967-021-07635-w

Darwish, S. M., & Darwish, I. M. (2022). Spectroscopic investigation of tau protein conformational changes by static magnetic field exposure. *Journal of Physics Communications*, *6*(7), Article 075004. https://doi.org/10.1088/2399-6528/ac7d3a

Deene, Y. D. (2022). Radiation dosimetry by use of radiosensitive hydrogels and polymers: Mechanisms, state-of-the-art and perspective from 3D to 4D. *Gels*, *8*(9), Article 599. https://doi.org/10.3390/gels8090599

Deene, Y. D. (2004). Essential characteristics of polymer gel dosimeters. *Journal of Physics: Conference Series*, *3*, 34–57. https://doi.org/10.1088/1742-6596/3/1/006

Farajollahi, A. R., Bonnett, D. E., Ratcliffe, A. J., Aukett, R. J., & Mills, J. A. (1999). An investigation into the use of polymer gel dosimetry in low dose rate brachytherapy. *The British Journal of Radiology*, *72*(863), 1085–1092. https://doi.org/10.1259/bjr.72.863.10700826

Gadagkar, S. R., & Call, G. B. (2015). Computational tools for fitting the hill equation to dose-response curves. *Journal of Pharmacological and Toxicological Methods*, *71*, 68–76. https://doi.org/10.1016/j.vascn.2014.08.006

Ishak, S. A., Iskandar, S. M., & Rahman, A. A. (2015). Sensitivity of HEMATEG induced by radiation dose in the diagnostic X-Ray energy range. *Advanced Materials Research*, *1087*, 267–271. https://doi.org/10.4028/www.scientific.net/AMR.1087.267

Jaszczak, M., Maras, P., & Kozicki, M. (2020). Characterization of a new N -vinylpyrrolidone-containing polymer gel dosimeter with Pluronic F-127 gel matrix. *Radiation Physics and Chemistry*, *177*, Article 109125. https://doi.org/10.1016/j.radphyschem.2020.109125

Javaheri, N., Yarahmadi, M., Refaei, A., & Aghamohammadi, A. (2020). Improvement of sensitivity of X-ray CT reading method for polymer gel in radiation therapy. *Reports of Practical Oncology & Radiotherapy*, *25*(1), 100–103. https://doi.org/10.1016/j.rpor.2019.12.017

Kipouros, P., Pappas, E., Baras, P., Hatzipanayoti, D., Karaiskos, P., Sakelliou, L., Sandilos, P., & Seimenis, I. (2001). Wide dynamic dose range of VIPAR polymer gel dosimetry. *Physics in Medicine and Biology*, *46*(8), 2143–2159. https://doi.org/10.1088/0031-9155/46/8/308

Kozicki, M., Berg, A., Maras, P., Jaszczak, M., & Dudek, M. (2020). Clinical radiotherapy application of N-vinylpyrrolidone-containing 3D polymer gel dosimeters with remote external MR-reading. *Physica Medica*, *69*, 134–146. https://doi.org/10.1016/j.ejmp.2019.11.014

Lotfy, S., Basfar, A. A., Moftah, B., & Al-Moussa, A. A. (2017). Comparative study of nuclear magnetic resonance and UV–visible spectroscopy dose-response of polymer gel based on N-(Isobutoxymethyl) acrylamide. *Nuclear Instruments and Methods in Physics Research, Section B: Beam Interactions with Materials and Atoms*, *413*, 42–50. https://doi.org/10.1016/j.nimb.2017.09.033

Masithoh, R. E., Pahlawan, M. F. R., Saputri, D. A. S., & Abadi, F. R. (2023). Visible-near-infrared spectroscopy and chemometrics for authentication detection of organic soybean flour. *Pertanika Journal of Science and Technology*, *31*(2), 671–688. https://doi.org/10.47836/pjst.31.2.03

Mustaqim, A. S., Yahaya, N. Z., Razak, N. N. A., & Zin, H. (2020). The dose enhancement of MAGAT gel dosimeter doped with zinc oxide at 6 MV photon beam. *Radiation Physics and Chemistry*, *172*, Article 108739. https://doi.org/10.1016/j.radphyschem.2020.108739

Nezhad, Z. A., & Geraily, G. (2022). A review study on application of gel dosimeters in low energy radiation dosimetry. *Applied Radiation and Isotopes*, *179*, Article 110015. https://doi.org/10.1016/j.apradiso.2021.110015

Nezhad, Z. A., Geraily, G., Parwaie, W., & Zohari, S. (2021). A novel investigation of the effect of different concentrations of methacrylic acid on the dose response of MAGAT gel dosimeter in intraoperative radiotherapy. *Radiation Physics and Chemistry*, *179*, Article 109214. https://doi.org/10.1016/j.radphyschem.2020.109214

Ozaki, Y. (2021). Infrared spectroscopy—mid-infrared, near-infrared, and far-infrared/terahertz spectroscopy. *Analytical Sciences*, *37*(9), 1193–1212. https://doi.org/10.2116/analsci.20R008

Pratiwi, R. A., Bayu, A., & Nandiyanto, D. (2022). How to read and interpret UV-VIS spectrophotometric results in determining the structure of chemical compounds. *Indonesian Journal of Educational Research and Technology*, *2*(1), 1–20. https://doi.org/10.17509/xxxx.vxix

Rabaeh, K. A., Hammoudeh, I. M. E., Oglat, A. A., Eyadeh, M. M., Abdel-Qader, A. J., Aldweri, F. M., & Awad, S. I. (2021). Polymer gel containing N,N′-methylene-bis-acrylamide (BIS) as a single monomer for radiotherapy dosimetry. *Radiation Physics and Chemistry*, *187*, Article 109522. https://doi.org/10.1016/j.radphyschem.2021.109522

Rashidi, A., Abtahi, S. M. M., Saeedzadeh, E., & Akbari, M. E. (2020). A new formulation of polymer gel dosimeter with reduced toxicity: Dosimetric characteristics and radiological properties. *Zeitschrift Für Medizinische Physik*, *30*(3), 185–193. https://doi.org/10.1016/j.zemedi.2020.02.002

Renner, I. E., & Fritz, V. A. (2020). Using near-infrared reflectance spectroscopy (NIRS) to predict glucobrassicin concentrations in cabbage and brussels sprout leaf tissue. *Plant Methods*, *16*(1), Article 136. https://doi.org/10.1186/s13007-020-00681-7

Shih, T. Y., Chen, W. T., Kuo, W. C., & Wu, J. (2022). Application of polarization-sensitive optical coherence tomography in measurement of gel dosimeters. *Journal of Medical and Biological Engineering*, *42*(5), 621–629. https://doi.org/10.1007/s40846-022-00711-w

Shukor, N. S. A., Musarudin, M., Abdullah, R., & Aziz, M. Z. A/ (2022). Dose distribution of 192Ir HDR brachytherapy source measurement using gafchromic® EBT3 film dosimeter and TLD-100H. *Pertanika Journal of Science and Technology*, *30*(1), 691–708. https://doi.org/10.47836/pjst.30.1.37

Watanabe, Y., Maeyama, T., Mizukami, S., Tachibana, H., Terazaki, T., Takei, H., Muraishi, H., Gomi, T., & Hayashi, S. I. (2022). Verification of dose distribution in high dose-rate brachytherapy for cervical cancer using a normoxic N-vinylpyrrolidone polymer gel dosimeter. *Journal of Radiation Research*, *63*(6), 838–848. https://doi.org/10.1093/jrr/rrac053

Zapata, F., López-Fernández, A., Ortega-Ojeda, F., Quintanilla, G., García-Ruiz, C., & Montalvo, G. (2021). Introducing ATR-FTIR spectroscopy through analysis of acetaminophen drugs: Practical lessons for interdisciplinary and progressive learning for undergraduate students. *Journal of Chemical Education*, *98*(8), 2675–2686. https://doi.org/10.1021/acs.jchemed.0c01231